EIT Images of Human Inspiration and Expiration using a D-bar Method with Spatial Priors

Melody Alsaker
Department of Mathematics
Gonzaga University
Spokane, Washington 92258
alsaker@gonzaga.edu

Jennifer L. Mueller
Department of Mathematics
School of Biomedical Engineering
Colorado State University
Fort Collins, Colorado 80523
mueller@math.colostate.edu

***Abstract*—The inclusion of a spatial prior in the high-frequency regime of the scattering transform for the 2-D D-bar method for electrical impedance tomography is studied for use with human subject data. The effects and balance of the two regularization parameters for the inverse problem are studied. Results on data from human volunteers reveal improved spatial resolution when compared to inspiratory and expiratory CT scans.**

I. INTRODUCTION

The inverse problem of electrical impedance tomography (EIT) is modeled by the generalized Laplace equation,

$$\nabla \cdot (\sigma(x,y)\nabla u(x,y)) = 0, \quad (x,y) \text{ in } \Omega, \tag{1}$$

where $\sigma(x,y)$ is the conductivity distribution to be reconstructed from boundary data represented by the Dirichlet-to-Neumann (DN) map,

$$\Lambda_\sigma : u|_{\partial\Omega} \mapsto \sigma \frac{\partial u}{\partial \nu}\Big|_{\partial\Omega}, \tag{2}$$

which physically takes boundary voltages to current densities on the boundary. It was established in [1] that for $\sigma \in C^2(\Omega)$, the DN map Λ_σ uniquely determines σ.

Cross-sectional EIT images of the chest have applications in bedside monitoring of patients with acute respiratory distress syndrome (ARDS), detection of pulmonary edema, atelectasis, and pneumothorax, since the heterogeneity characterizing these disorders is well-represented in a 2-D slice in a patient lying down. The references [2], [3] provide surveys of clinical pulmonary applications of EIT.

The inverse problem of EIT is severely ill-posed, and hence highly sensitive to measurement noise and modeling errors. As a result, EIT reconstructions tend to suffer from low spatial resolution. The use of prior information in the reconstruction process is a classic approach in inverse problems to regularize and improve spatial resolution. Iterative reconstruction methods include *a priori* information about the conductivity distribution in the chest in the regularization term (see, for example, [4]–[15].) In this work, the conductivity is computed using a direct (non-iterative) method known as the *D-bar* method.

D-bar reconstruction methods are based on special functions known as complex geometrical optics (CGO) solutions, which satisfy a direct relationship to the unknown conductivity, and through the computation of the CGO solutions from measured EIT data, the inverse problem can be solved directly (non-iteratively). A real-time implementation of the D-bar method was given in [16], and the D-bar method has been used as the reconstruction method in a study to estimate regions of air trapping in cystic fibrosis patients [17] and in a study of EIT-derived measures of spirometry [18]. Patients with cystic fibrosis receive a CT scan approximately every three years (more often if clinically indicated). This offers the opportunity to use some information about the patient's anatomy from the CT scan as priors in the reconstruction algorithm. A method for including a spatial prior in the D-bar reconstruction algorithm was first proposed in [19] and tested on simulated data. In [20] a method for optimizing the spatial prior was presented for use with experimental tank data. In this work we demonstrate the effectiveness of that method on data collected on several patients with cystic fibrosis during tidal breathing. CT scans of the patients' chests were available as part of their regular clinical visit and were used to construct the priors.

II. METHODS

A. Outline of the D-bar Method (No Priors)

The D-bar method applied here is based on the global uniqueness proof for the 2-D inverse conductivity problem [1] and subsequent implementation and development (see [21] and the references therein). The CGO solutions are special solutions to the Schrödinger equation, which arises from the change of variables in (1) $\tilde{u} = \sqrt{\sigma}u$ and $q = \sigma^{-1/2}\Delta\sigma^{1/2}$:

$$(-\Delta + q(x,y))\tilde{u}(x,y) = 0, \quad (x,y) \in \Omega. \tag{3}$$

Introducing a a non-physical complex frequency k in (3), extending the equation to $(x,y) \in \mathbb{R}^2$, and identifying a point in the complex plane $z = x + iy$ with the spatial point (x,y), the CGO solutions $\psi(z,k)$ satisfy,

$$(-\Delta + q(z))\psi(z,k) = 0, \quad z \in \mathbb{R}^2. \tag{4}$$

The related CGO solution $\mu(z,k)$ is defined by $\mu \equiv e^{ikz}\psi(z,k)$. The CGO solution $\psi(z,k)$ is related to the DN map, and hence the measured data, through the boundary integral equation,

$$\psi(z,k)|_{\partial\Omega} = e^{ikz}|_{\partial\Omega} - \int_{\partial\Omega} G_k(z-\zeta)(\Lambda_\sigma - \Lambda_1)\psi(\cdot,k)ds,$$

Submitted On: October 4, 2018
Accepted On: October 21, 2018

where G_k is the Faddeev's Green's function for the Laplacian operator [22], and Λ_1 denotes the DN map corresponding to $\sigma \equiv 1$ in Ω. The conductivity can be directly computed from knowledge of $\mu(z,k)$ in the interior of Ω through,

$$\sigma(z) = \mu^2(z,0).$$

To compute μ in the interior, the scattering transform $\mathbf{t}(k)$ of the conductivity is needed, and an integral equation is solved for μ:

$$\mu(z,k) = 1 + \frac{1}{(2\pi)^2} \int_{\mathbb{R}^2} \frac{\mathbf{t}(k')}{\overline{k'}(k-k')}\, e^{-i(kz+\bar{k}\bar{z})}\overline{\mu(z,k')}dk',$$

where the scattering transform is a nonphysical nonlinear Fourier transform of q defined by,

$$\mathbf{t}(k) := \int_{\Omega} e^{i\bar{k}\bar{z}} q(z)\psi(z,k)dz. \tag{5}$$

Since q is unknown, in practice the scattering transform is computed from the data via the formula,

$$\mathbf{t}(k) = \int_{\partial\Omega} e^{i\bar{k}\bar{z}} (\Lambda_\sigma - \Lambda_1)\psi(z,k)ds. \tag{6}$$

Difference images from a reference frame in which the voltage on each electrode was averaged over all of the frames in the data collection sequence can be computed using $\mathbf{t}^{\exp}_{\text{dif}}(k)$, introduced in [23], where the CGO solution $\psi(z,k)$ is replaced by its asymptotic behavior e^{ikz} in the scattering transform. This approximation is denoted by $\mathbf{t}^{\exp}_{\text{dif}}(k)$ and is given by,

$$\begin{aligned} \mathbf{t}^{\exp}_{\text{dif}}(k) \;&\equiv\; \int_{\partial\Omega} e^{i\bar{k}\bar{z}}(\Lambda_\sigma - \Lambda_1)e^{ikz}ds(z) \\ &-\; \int_{\partial\Omega} e^{i\bar{k}\bar{z}}(\Lambda_{\text{ref}} - \Lambda_1)e^{ikz}ds(z), \\ &=\; \int_{\partial\Omega} e^{i\bar{k}\bar{z}}(\Lambda_\sigma - \Lambda_{\text{ref}})e^{ikz}ds(z) \end{aligned}$$

where Λ_{ref} is the DN map corresponding to the averaged data.

B. Outline of the D-bar Method with Spatial Priors

Since the computation of the scattering transform blows up in the presence of noise outside $|k| \le R_1$ for some R_1, as in [19] the scattering transform is extended to a larger k disk by computing it for the noise-free case of a known conductivity and by using the definition of the scattering transform (5), rather than the equation utilizing the data (6); this scattering transform is denoted $\mathbf{t}_{\text{pr}}$. This leads to a piecewise-defined scattering transform $\mathbf{t}_{\text{pw}}$, where the prior information is encoded in the method in the high-frequency components of the scattering transform through $\mathbf{t}_{\text{pr}}$:

$$\mathbf{t}_{\text{pw}}(k) := \begin{cases} \mathbf{t}^{\exp}_{\text{dif}}(k), & |k| \le R_1 \\ \mathbf{t}_{\text{pr}}(k), & R_1 < |k| \le R_2 \\ 0, & |k| > R_2 \end{cases}. \tag{7}$$

The prior information is included in a second location in the computations as well. Denoting the CGO solution computed for the noise-free case of a known conductivity by,

$$\mu_{\text{int}}(z) := \frac{1}{\pi R_2^2} \int_{|k|\le R_2} \mu_{\text{pr}}(z,k)dk, \tag{8}$$

we solve a modified integral equation:

$$\begin{aligned} &\mu_{R_2,\alpha}(z,k) = \alpha + (1-\alpha)\mu_{\text{int}}(z) \\ &+ \frac{1}{(2\pi)^2}\int_{|k|\le R_2} \frac{\mathbf{t}_{\text{pw}}(k')}{\bar{k}'(k-k')} e_{-k'}\overline{\mu_{R_2,\alpha}(z,k')}\, dk', \end{aligned} \tag{9}$$

where the weighting parameter α is used to control the influence of the term μ_{int} upon the resulting reconstruction.

C. Construction of the Spatial Prior

The prior consists of a simple phantom representative of known features of the true conductivity distribution with assigned conductivity values. In this work, the inspiratory and expiratory CT scans best representing the slice of the chest in the plane of the electrodes were chosen to construct two sets of priors – one for inspiration and one for expiration. The boundaries of the chest shape, lungs, and heart, were approximated from the CT scans by importing the images into MATLAB and using the tool for exporting selected coordinates (r_n, θ_n) in the image to a text file. Fourier series approximations to the chest shape and the organ boundaries are represented by the function $r(\theta)$:

$$r(\theta) = a_0 + \sum_{i=1}^{N} a_i\cos(\theta) + b_i\sin(\theta),$$

where $\{a_i\}_{i=0}^N$ and $\{b_j\}_{j=1}^N$ are chosen so as to minimize the root mean squares error $\|r(\theta_n) - r_n\|$ over all the selected coordinates (r_n, θ_n).

Denoting the vector of conductivity values in each of the regions (heart, left lung, right lung, and background) by $\mathbf{c}$, we seek to find a $\mathbf{c}$ that minimizes the difference between the scattering transform computed from the measured data $\mathbf{t}^{\text{vec}}$ and the scattering transform computed from the prior $\mathbf{t}^{\text{vec}}_{\text{pr}}$. We define the objective function,

$$J(\mathbf{c}) := \|\mathbf{t}^{\text{vec}}_{\text{pr}}(\mathbf{c}) - \mathbf{t}^{\text{vec}}\|^{\mathbf{2}}_{\mathbf{2}}, \tag{10}$$

and solve the constrained nonlinear minimization problem,

$$\underset{\mathbf{c}\in\mathbb{R}^\mathbf{n}}{\text{minimize}}\ J(\mathbf{c}) \ \text{ subject to } \ell \le \mathbf{c} \le u, \tag{11}$$

where ℓ and u are n-vectors of lower and upper bounds, using the Interior Point Algorithm in MATLAB's Optimization Toolbox.

III. Results and Discussion

This data was collected with the ACE1 EIT system [24] as part of a larger study conducted in accordance with the amended Declaration of Helsinki. Data were collected at Children's Hospital Colorado, Aurora, CO under the approval of the Colorado Multiple Institutional Review Board (COMIRB) (approval number COMIRB 14-0652). Informed written parental consent and children's informed assent was obtained from the subjects. The data used in this paper are from a 6 year old human male cystic fibrosis patient (referred to here as Subject 1) and a 12 year old human female cystic fibrosis patient (referred to here as Subject 2). The CT scans were performed as part of the subject's standard care, and the EIT data was collected immediately prior to the CT scan.

Pediatric EKG electrodes (Phillips 13951C) of height 33 mm and width 23 mm were placed around the perimeter of the subject's chest with an additional electrode on the shoulder as ground. The number of electrodes used was the maximum number that would fit around the circumference with no electrodes touching. For Subject 1, this was 22 electrodes, and for Subject 2 this was 24 electrodes. Alternating currents with frequency 125 kHz were applied at approximately 4 mA, peak-to-peak using pairwise adjacent excitation patterns. After the EIT data was collected, fiducial markers were placed at the center of each electrode, so that their locations could be noted in the CT scans. The expiratory CT scan with the most electrodes in the plane of the scan was chosen for creating the boundary and prior for full expiration, and the inspiratory scan at the level closest to the chosen expiratory CT scan was chosen for creating the boundary and prior for full inspiration. It should be noted that the expiratory CT scans are 4 cm apart in the Z (caudal-cranial) direction, while the inspiratory scans are 0.5 mm apart in the Z-direction.

Approximate organ boundaries and the outer boundary were visually extracted from the CT scan, and the domain was divided into four regions: background, heart, left lung, and right lung. The spatial priors for Subject 1 for inspiration and expiration are found in Fig. 2, and the spatial priors for Subject 2 for inspiration and expiration are found in Fig. 5. Initial guesses for the conductivity in each of the four regions were chosen from a preliminary reconstruction, and the constrained optimization problem (11) was solved to obtain values for the prior in each of the four regions. The scattering transform $\mathbf{t}_{\rm pr}$ was then computed, and the scattering transform (7) was used for the final reconstruction. Figs. 9 and 10 show the real and imaginary parts of the scattering transforms $\mathbf{t}_{\rm pr}$, which are computed from equation (5) using the spatial priors with the optimized organ values, and the real and imaginary parts of the scattering transforms $\mathbf{t}_{\rm pw}$, which are computed from equation (7), which pieces together $\mathbf{t}_{\rm dif}^{\rm exp}$ computed from the data and $\mathbf{t}_{\rm pr}$. All plots are on $|k| \leq 6$ (i.e., $R_2 = 6$ for $\mathbf{t}_{\rm pw}$), and it is evident that there is some mismatch in amplitude and features of $\mathbf{t}_{\rm dif}^{\rm exp}$ with $\mathbf{t}_{\rm pw}$. A more thorough study of the effect of this mismatch is a topic of future work.

The CT scan slices at inspiration and expiration from the two subjects are shown in Figs. 1 and 4 in the standard DICOM orientation, in which the subject's left is on the viewer's right. The expiratory CT scan for the 6 year old subject includes some diaphragm in the subject's right lung, which raises the question of whether the diaphragm is expected to be visible in the EIT images.

The EIT reconstructions effectively compute the conductivity within a 3-D slice of the body with a thickness equal

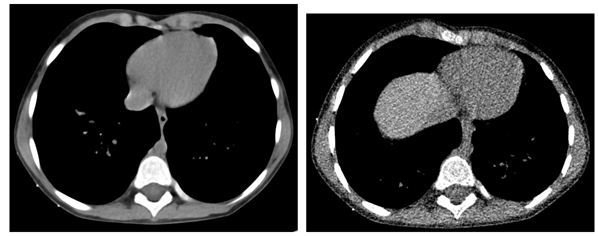

Fig. 1. Inspiratory (left) and expiratory (right) CT scans of a 6-year old male subject used to construct the boundary shape and organs for the spatial priors.

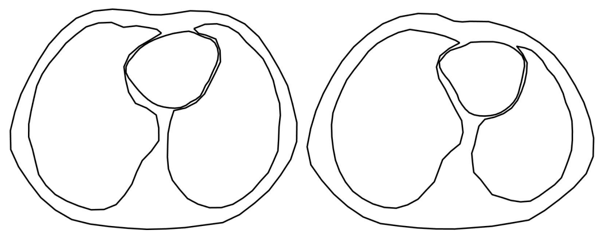

Fig. 2. Inspiratory (left) and expiratory (right) approximate organ boundaries used in the *a priori* D-bar method for a 6-year old male subject.

to that of the electrodes in the cross-section defined by the placement of the row of electrodes. The thickness of the slice is approximate, since in the clinical setting the centers of the electrodes are not aligned perfectly in a plane, and the slice that they define may well be a skew from the CT scan slices. Furthermore, the induced currents will flow out of the plane of the electrodes and affect the reconstructions. The effect of out-of-plane currents on EIT images has been analyzed in, for example, [25]–[28], and the influence of out-of-plane inhomogeneities is dependent on the conductivity of the inhomogeneities and their radial distance from the electrodes, with the least influence in the center of the slice [25]. One rule of thumb is that out-of-plane objects lying a vertical distance within 1/2 the radius R of the domain may influence the voltage measurements [28]. Approximating R by $P/(2\pi)$, where P is the perimeter of the subject in the plane of the majority of the electrodes, which for this subject was $P = 62$ cm, $R/2 = P/(4\pi) \approx 4.9$ cm. While the CT scan slice at $Z = 141$ mm contains the most fiducial markers, several markers can also be seen in the slice in Fig. 1, which is at $Z = 161$ mm, and so the effect of the diaphragm on the reconstructed images is inconclusive from this analysis. Another point to consider is the fact that the position of the diaphragm changes when a patient is supine, as is the case in the CT scanner, versus when they are sitting up, as is the case when the EIT data was collected [29]. In [29] MRI images were collected on 10 healthy men in both the sitting and supine positions, and it was found that the movement of the diaphragm (known as the diaphragmatic excursion) was greater in the supine position than in the sitting position. Since these factors do not point strongly to an influence of the presence of the diaphragm on the reconstructions, the diaphragm was not included in the prior in this study.

Reconstructions from inspiratory and expiratory data of

Subjects 1 and 2 are shown in Figs. 3 and 6, respectively. Regions of high relative conductivity are shown in red, and regions of low relative conductivity are plotted in blue. To demonstrate the effects of the parameters R_2 and α on the reconstructions, comparison plots for the inspiratory scans from both subjects are shown in Figs. 7 and 8. For all reconstructions here, $R_1 = 5$, so a prior with $R_2 = 6$ is fairly weak. Note that a stronger prior (indicated by larger R_2 or smaller α) does not necessarily improve the reconstruction further, and may in fact introduce artifacts. This is likely due to increased mismatch between the *a priori* scattering transform $\mathbf{t}_{\mathrm{pr}}$ and the scattering transform computed from the measured data.

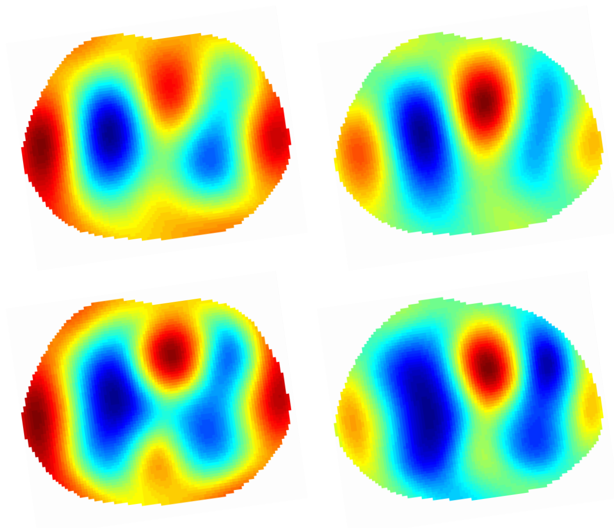

Fig. 3. Top: Standard D-bar reconstructions of data collected during inspiration (left) and expiration (right) for a 6-year-old male subject. Bottom: Corresponding D-bar reconstructions with optimized prior.

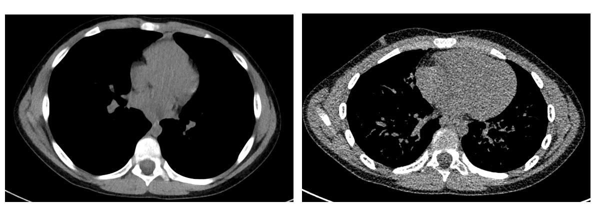

Fig. 4. Inspiratory (left) and expiratory (right) CT of 12-year old female subject used to construct the boundary shape and organs for the spatial priors.

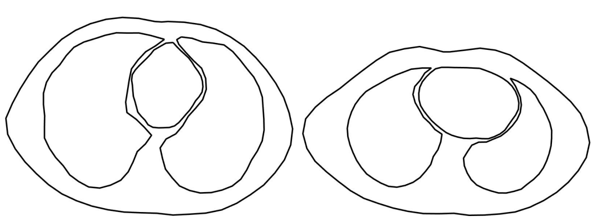

Fig. 5. Inspiratory (left) and expiratory (right) approximate organ boundaries used in the *a priori* D-bar method for a 12-year old female subject.

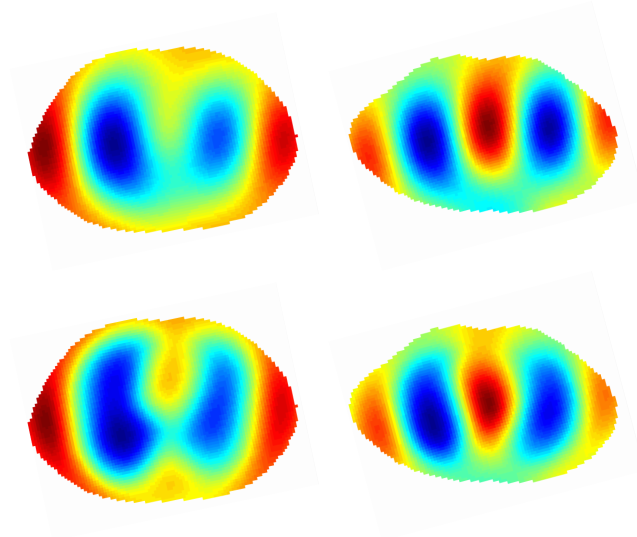

Fig. 6. Top: Standard D-bar reconstructions of data collected during inspiration (left) and expiration (right) for a 12-year-old female subject. Bottom: Corresponding D-bar reconstructions with optimized prior.

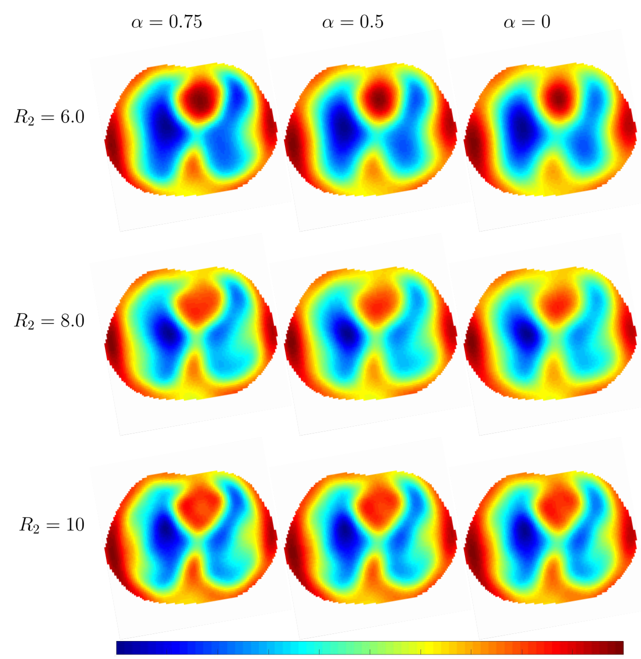

Fig. 7. A comparison of D-bar reconstructions of inspiratory data from a 6-year-old male subject using a prior with various values of R_2 and α.

IV. Conclusion

Spatial resolution of the EIT images reconstructed by the D-bar method is improved through the use of simple spatial priors. Further research is needed to determine their clinical value and whether they aid in detecting pathologies.

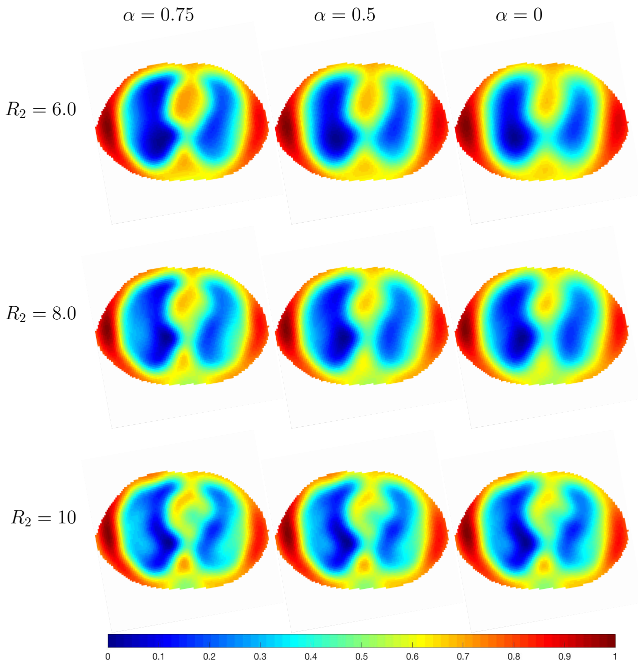

Fig. 8. A comparison of D-bar reconstructions of inspiratory data from a 12-year-old female subject using a prior with various values of R_2 and α.

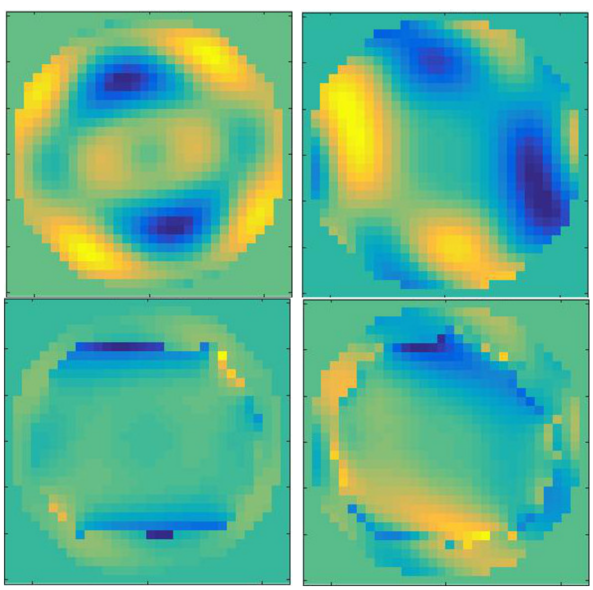

Fig. 9. Top: Plots of the real (left) and imaginary (right) parts of the *a priori* scattering transform $\mathbf{t}_{\mathrm{pr}}$ using truncation radius $R_2 = 6$, for an inspiratory frame from a 6-year-old male subject. Bottom: Real and imaginary parts of the corresponding piecewise-defined scattering transform $\mathbf{t}_{\mathrm{pw}}$.

Acknowledgment

This project was supported by award 1R21EB016869-01 from the NIBIB. The content is solely the responsibility of the authors and does not necessarily represent the official view of the NIBIB or NIH.

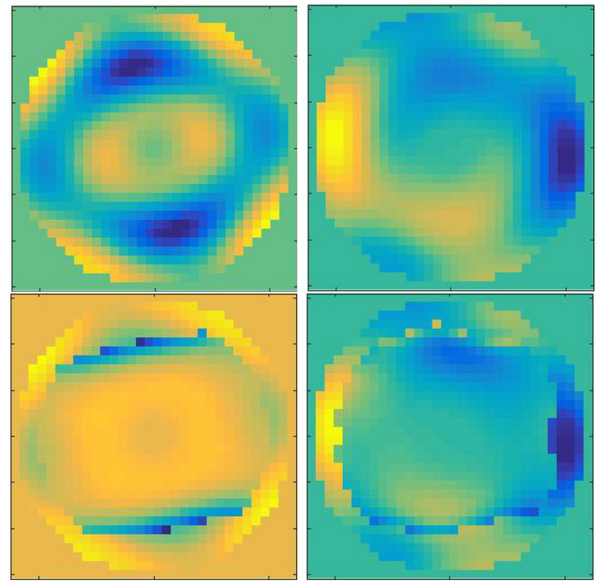

Fig. 10. Top: Plots of the real (left) and imaginary (right) parts of the *a priori* scattering transform $\mathbf{t}_{\mathrm{pr}}$ using truncation radius $R_2 = 6$, for an inspiratory frame from a 12-year-old female subject. Bottom: Real and imaginary parts of the corresponding piecewise-defined scattering transform $\mathbf{t}_{\mathrm{pw}}$.

References

[1] A. I. Nachman, "Global uniqueness for a two-dimensional inverse boundary value problem," Ann. Math., vol. 143, no. 1, pp. 71–96, 1996.

[2] E. Costa, R. Gonzalez Lima, and M. Amato, "Electrical impedance tomography," in Intensive Care Medicine (J. Vincent, ed.), pp. 394–404, Springer, New York, 2009.

[3] D. Nguyen, J. C. Thiagalingam, and A. A. McEwan, "A review on electrical impedance tomography for pulmonary perfusion imaging," Physiol. Meas., vol. 33, no. 5, pp. 695–706, 2012.

[4] N. J. Avis and D. C. Barber, "Incorporating a priori information into the Sheffield filtered backprojection algorithm," Physiol. Meas., vol. 16, no. 3A, pp. A111–A122, 1995.

[5] U. Baysal and B. M. Eyüboglu, "Use of a priori information in estimating tissue resistivities - a simulation study," Phys. Med. and Biol., vol. 43, no. 12, pp. 3589–3606, 1998.

[6] E. D. L. B. Camargo, "Development of an absolute electrical impedance imaging algorithm for clinical use," PhD thesis, University of São Paulo, 2013.

[7] H. Dehghani, D. C. Barber, and I. Basarab-Horwath, "Incorporating a priori anatomical information into image reconstruction in electrical impedance tomography," Physiol. Meas., vol. 20, no. 1, pp. 87–102, 1999.

[8] D. C. Dobson and F. Santosa, "An image-enhancement technique for electrical impedance tomography," Inverse Probl., vol. 10, no. 2, pp. 317–334, 1994.

[9] D. Ferrario, B. Grychtol, A. Adler, J. Sola, S. H. Bohm, and M. Bodenstein, "Toward morphological thoracic EIT: Major signal sources correspond to respective organ locations in CT," IEEE T. Med. Imaging, vol. 59, no. 11, pp. 3000–3008, 2012.

[10] D. Flores-Tapia and S. Pistorius, "Electrical impedance tomography reconstruction using a monotonicity approach based on a priori knowledge," in Engineering in Medicine and Biology Society (EMBC), 2010 Annual International Conference of the IEEE, pp. 4996–4999, Aug. 2010.

[11] J. P. Kaipio, V. Kolehmainen, M. Vauhkonen, and E. Somersalo, "Inverse problems with structural prior information," Inverse Probl., vol. 15, no. 3, p. 713, 1999.

[12] K. Y. Kim, S. I. Kang, M. C. Kim, S. Kim, Y. J. Lee, and M. Vauhkonen, "Dynamic image reconstruction in electrical impedance tomography with known internal structures," IEEE Transactions on Magnetics, vol. 38, pp. 1301–1304, Mar. 2002.

[13] F. S. Moura, J. C. C. Aya, A. T. Fleury, M. B. P. Amato, and R. G. Lima, "Dynamic imaging in electrical impedance tomography of the human chest with online transition matrix identification," IEEE Transactions on Biomedical Engineering, vol. 57, pp. 422–431, Feb. 2010.

[14] M. Soleimani, "Electrical impedance tomography imaging using a priori ultrasound data," BioMed. Eng. OnLine, vol. 5, no. 8, 2006.

[15] M. Vauhkonen, D. Vadasz, P. A. Karjalainen, E. Somersalo, and J. P. Kaipio, "Tikhonov regularization and prior information in electrical impedance tomography," IEEE T. Med. Imaging, vol. 17, no. 2, pp. 285–293, 1998.

[16] M. Dodd and J. Mueller, "A real-time D-bar algorithm for 2-D electrical impedance tomography data," Inverse Probl. Imag., vol. 8, no. 4, pp. 1013–1031, 2014.

[17] J. Mueller, P. Muller, M. Mellenthin, E. DeBoer, R. Murthy, M. Capps, M. Alsaker, R. Deterding, and S. Sagel, "A method of estimating regions of air trapping from electrical impedance tomography data," Physiological Measurement, vol. 39, no. 5, p. 05NT01, 2018.

[18] P. Muller, J. Mueller, M. Mellenthin, R. Murthy, M. Capps, B. Wagner, M. Alsaker, R. Deterding, S. Sagel, and J. Hoppe, "Evaluation of surrogate measures of pulmonary function derived from electrical impedance tomography data in children with cystic fibrosis," Physiological Measurement, vol. 39, no. 4, p. 045008, 2018.

[19] M. Alsaker and J. Mueller, "A D-bar algorithm with a priori information for 2-dimensional electrical impedance tomography," SIAM J. Imaging Sci., vol. 9, no. 4, pp. 1619–1654, 2016.

[20] M. Alsaker and J. L. Mueller, "Use of an optimized spatial prior in d-bar reconstructions of EIT tank data," In review, 2017.

[21] J. L. Mueller and S. Siltanen, Linear and Nonlinear Inverse Problems with Practical Applications. Philadelphia, PA: SIAM, 2012.

[22] L. D. Faddeev, "Increasing solutions of the schroedinger equation," Sov. Phys. Dokl., vol. 10, pp. 1033–1035, 1966.

[23] D. Isaacson, J. L. Mueller, J. C. Newell, and S. Siltanen, "Imaging cardiac activity by the D-bar method for electrical impedance tomography," Physiol. Meas., vol. 27, no. 5, pp. S43–S50, 2006.

[24] M. Mellenthin, J. Mueller, E. de Camargo, F. de Moura, T. Santos, R. Lima, S. Hamilton, P. Muller, and M. Alsaker, "The ACE1 electrical impedance tomography system for thoracic imaging," IEEE Transactions on Instrumentation and Measurement, p. to appear, 2018.

[25] B. M. Eyuboglu, B. H. Brown, and D. C. Barber, "Limitations to SV determination from APT images," in Images of the Twenty-First Century. Proceedings of the Annual International Engineering in Medicine and Biology Society, pp. 442–443 vol. 2, Nov. 1989.

[26] R. Guardo, C. Boulay, B. Murray, and M. Bertrand, "An experimental study in electrical impedance tomography using backprojection reconstruction," IEEE Transactions on Biomedical Engineering, vol. 38, pp. 617–627, July 1991.

[27] K. S. Rabbani and A. M. B. H. Kabir, "Studies on the effect of the third dimension on a two-dimensional electrical impedance tomography system," Clinical Physics and Physiological Measurement, vol. 12, no. 4, p. 393, 1991.

[28] R. S. Blue, D. Isaacson, and J. C. Newell, "Real-time three-dimensional electrical impedance imaging," Physiological Measurement, vol. 21, no. 1, p. 15, 2000.

[29] R. Takazakura, M. Takahashi, N. Nitta, and K. Murata, "Diaphragmatic motion in the sitting and supine positions: Healthy subject study using a vertically open magnetic resonance system," Journal of Magnetic Resonance Imaging, vol. 19, no. 5, pp. 605–609, 2004.